Reviewed research article

Geodetic mass balance of Mýrdalsjökull ice cap, 1999–2021

Maud Bernat[1], Joaquín M. C. Belart[2], Etienne Berthier[1], Tómas Jóhannesson[3], Romain Hugonnet[1,4], Amaury Dehecq[5], Eyjólfur Magnússon[6] and Andri Gunnarsson[7]

[1]*Université de Toulouse, LEGOS (CNES/CNRS/IRD/UT3), Toulouse, France*

[2]*National Land Survey of Iceland, Akranes, Iceland*

[3]*Icelandic Meteorological Office, Reykjavík, Iceland* [4]*University of Washington, Seattle, USA*

[5]*Laboratoire de Glaciologie et Géophysique de l'Environnement, Grenoble, France*

[6]*Institute of Earth Sciences, University of Iceland* [7]*Landsvirkjun, the National Power Company of Iceland*

Corresponding author maud.bernat@univ-tlse3.fr; https://doi.org/10.33799/jokull2023.73.035

Abstract — *The mass balance of Mýrdalsjökull, the fourth largest Icelandic ice cap (520 km^2 in 2019), has received less attention so far than the mass balance of the three largest ice caps, Vatnajökull, Hofsjökull and Langjökull. Here, we used digital elevation models (DEMs) derived from the untapped SPOT5 archive (2003−2014), lidar data (2010), Pléiades imagery (2014−2021), aerial photographs from 1999 and the ArcticDEM dataset (2010−2018) to estimate the mass balance of Mýrdalsjökull. A pre-processing of the DEMs was first performed: co-registration, filtering and void interpolation. Then, applying a Gaussian Process (GP) regression, a spatially and temporally continuous elevation dataset was created, in 15×15 m resolution and 30-day increments over the time span 1999 to 2021. Volume and mass changes based on the GP-interpolated elevation dataset were computed and analysed in 5- to 6-year intervals between 1999 and 2021. An average mass balance of -1.23 ± 0.10 m w.e. a^{-1} was estimated for this time period, with a trend towards a less negative mass balance from -1.83 ± 0.13 m w.e. a^{-1} (1999−2005) to -0.41 ± 0.03 m w.e. a^{-1} (2016−2021). An analysis of three climatically different catchments of Mýrdalsjökull showed a significant spatial variability in the estimated mass balance but a similar temporal variation.*

INTRODUCTION

Glaciers are retreating worldwide and mass-loss rates have accelerated in response to global warming in recent decades (IPCC 2019, 2021; Pörtner *et al.*, 2019). This evolution affects the environment in many ways, such as raising global sea level or changing the hydrology of areas adjacent to glaciers. Lateral support of adjacent hillsides may be reduced when glacier surfaces are lowered, leading to an increase in landslide activity. Glacier downwasting may also increase natural hazards due to jökulhlaups from marginal lakes because of changing conditions near the ice margin where lakes can form at new locations. Between 2000 and 2019, the global glacier mass loss outside of the polar ice sheets was estimated as 267 ± 16 Gt a^{-1}, which corresponds to $21 \pm 3\%$ of the observed sea-level rise over the same time period (Hugonnet *et al.*, 2021). To investigate the relationship between glacier changes and climate and better predict future evolution, spatially and temporally detailed measurements must be carried out. Thanks to remote sensing methods developed over the last decades, common problems associated with mass-balance measurements based on field observations (costs, accessibility, spatial extent) have been overcome. DEMs created from spaceborne and airborne platforms can now be used to produce geodetic mass-balance estimates for entire glaciers and enable the production of regional and global estimates of glacier mass loss e.g., Berthier *et al.* (2023); Hugonnet *et al.* (2021).

Temperate glaciers cover 10% of the area of Iceland (Björnsson and Pálsson, 2008), and they contained $\sim$3400 km^3 of ice in 2019 (Aðalgeirsdóttir *et al.*, 2020) corresponding to a potential sea-level rise of 9 mm if melted. Icelandic ice caps are characterized by a large variability on decadal time scales related to climate variations and, to a lesser extent, to volcanic activity (Björnsson and Pálsson, 2008). Despite intermittent periods of close to zero mass balance, such as in the 1980s, Icelandic glaciers have mostly been retreating since the end of the Little Ice Age, around 1890 (Hannesdóttir *et al.*, 2020). The total mass loss during the period $\sim$1890 to 2019 was estimated to be -540 ± 130 Gt, half of which took place during 1994$-$2019 (Aðalgeirsdóttir *et al.*, 2020). The accelerated retreat of Icelandic glaciers has already led to a variety of impacts on water resources (Jóhannesson *et al.*, 2007), hydropower (Sveinsson *et al.*, 2016), natural hazards and tourism (Björnsson *et al.*, 2018).

The three largest ice caps in Iceland, Vatnajökull, Hofsjökull and Langjökull, represent 90% of the total glacier area (Hannesdóttir *et al.*, 2020). Consequently, most glaciological studies have focused on these glaciers. Glaciological mass-balance measurements have been carried out seasonally for $\sim$30 years (Björnsson and Pálsson, 2008; Thorsteinsson *et al.*, 2017) on all three ice caps and numerous remote-sensing studies of changes of Vatnajökull (e.g., Hannesdóttir *et al.*, 2015), Hofsjökull (e.g., Thorsteinsson *et al.*, 2017) and Langjökull (e.g., Pálsson, 2012) have been performed. Mass-balance surveys have also been conducted annually on Mýrdalsjökull, the fourth largest Icelandic ice cap, since 2007 at three to five locations, mainly in the accumulation area (Ágústsson *et al.*, 2013). In the ablation area, the mass balance at ca. 1000 m a.s.l. of the N-flowing outlet glacier Sléttjökull has been estimated from horizontal displacement of the tephra layer from the 1918 eruption of Katla (Mayer *et al.*, 2017; Hagg *et al.*, 2023). However, it has not been possible to derive glacier-wide mass balance for Mýrdalsjökull as the measurement sites are few and not well distributed (locations shown in Ágústsson *et al.*, 2013). Digital elevation models created from spaceborne and airborne platforms provide an opportunity to produce a geodetic mass-balance estimate for Mýrdalsjökull and to compare it with the other large Icelandic ice caps. Belart *et al.* (2020) estimated the geodetic mass balance of the ice cap from 1960 to 2010 over decadal time spans. However, the temporal sampling of remote-sensing data available before 2010 does not allow capturing the variability at shorter temporal scales. The untapped high-resolution SPOT5 (Korona *et al.*, 2009), Pléiades (Berthier *et al.*, 2014) and ArcticDEM (Porter *et al.*, 2018) datasets cover Mýrdalsjökull with almost annual temporal resolution over the past two decades and offer an opportunity to analyse the changes of the ice cap in much more detail than previously possible.

The goal of this study is to process high-resolution DEMs using state-of-the-art methods and produce geodetic mass-balance estimates for Mýrdalsjökull in the period 1999$-$2021. These results are then used to quantify and analyse spatial and temporal trends, and the variability of the mass balance.

STUDY REGION AND DATASETS

In 2019, the area of Mýrdalsjökull was 520 km^2 (Hannesdóttir *et al.*, 2020). The total volume and average ice thickness in 2000 were estimated as $\sim$140 km^3 and $\sim$230 m, respectively (Björnsson *et al.*, 2000; Björnsson and Pálsson, 2008). Located 15 km from the south coast of Iceland, the glacier is exposed to a maritime climate. Low-pressure systems that recurrently hit the south coast make this region the wettest in Iceland (Crochet, 2007).

The ice cap topography rises from 100 m a.s.l. at the terminus of Sólheimajökull up to 1493 m a.s.l. at Goðabunga (elevations measured in 2021, Figure 1a). The largest part of the accumulation area is a gently sloping plateau between 1300 and 1350 m a.s.l. It is surrounded by a caldera rim with some nunataks emerging 100 m to 200 m above the central zone. Several outlet glaciers, including Entujökull, Sléttjökull and Öldufellsjökull in the north, Sandfellsjökull in the east, Kötlujökull in the southeast, Sólheimajökull and Goðalandsjökull in the south and southwest, and Tungnakvíslarjökull in the west, are fed by ice flow from the accumulation area.

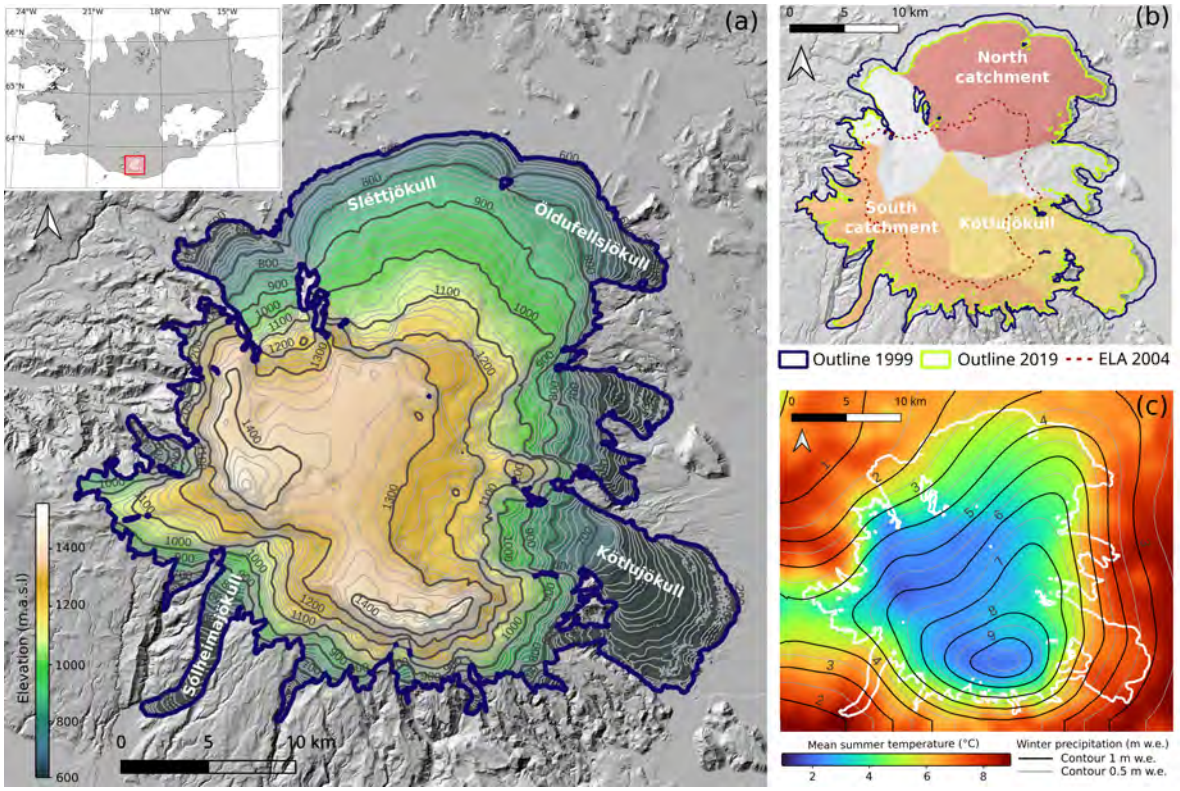

Figure 1. Study site and average climatic conditions. (a) DEM of Mýrdalsjökull from ÍslandsDEMv1, https://dem.lmi.is and the corresponding contour map (contour interval of 100 m in black, 20 m in grey). The names of the main outlets are indicated in white. (b) Mýrdalsjökull glacier outlines in 1999 and 2019 and definition of the main ice-flow catchments (north, south and Kötlujökull). The equilibrium-line altitude (ELA), which is approximated as the snowline derived from a 2004-10-05 SPOT5 orthoimage (Belart *et al.* 2020), is indicated as a red dashed line. (c) Average climatic conditions between 1999 and 2019: mean summer temperature (computed as the mean for the period May 21st to September 30th each year) is shown in the background. Total winter precipitation (calculated as the sum from October 1st of the previous year to May 20th each year) is displayed as contours in meters w.e. per year. The temperature dataset was extracted from Crochet *et al.* (2011, updated) and the precipitation dataset comes from the HARMONIE numerical model (Nawri *et al.*, 2017; Bengtson *et al.* 2017). – *Yfirlitskort af Mýrdalsjökli og veðurfarsskilyrðum. (a) Landlíkan úr ÍslandsDEMv1 https://dem.lmi.is með hæðarlínum (100 m línur svartar, 20 m línur gráar). Nöfn helstu skriðjökla eru sýnd með hvítu letri. (b) Útlínur jökulsins 1999 og 2019 og helstu ísflæðisvið (norðurhluti, suðurhluti og Kötlujökull). Jafnvægislína (ELA) byggð á uppréttri SPOT5 gervitunglamynd frá 2004-10-05 er sýnd með slitinni rauðri línu. (c) Veðurfar tímabilsins 1999 til 2019: meðalhiti sumars (meðaltal tímabilsins 21. maí til 30. sept. hvert ár) er sýndur í bakgrunni, og vatnsgildi vetrarúrkomu (summa frá 1. okt. fyrra árs til 1. maí hvert ár) með jafngildislínum. Hitagögnin eru frá Crochet o.fl. (2011, uppfært) og úrkomugögnin eru skv. niðurkvörðun með HARMONIE veðurlíkaninu (Nawri o.fl., 2017; Bengtson o.fl., 2017).*

The active subglacial volcano Katla is located under Mýrdalsjökull. The caldera covers a roughly circular area of ∼100 km^2 under the central part of the glacier, with up to ∼750 m thick ice (Björnsson *et al.*, 2000; Magnússon *et al.*, 2021). The eruption frequency is estimated to be around once every 40 to 80 years (Gudmundsson *et al.*, 2008). The last eruption took place in 1918. However, the geothermal activity clearly manifests itself by the presence of surface depressions referred to as "ice cauldrons" at many locations on the glacier. The geothermally induced ice cauldrons are a source of jökulhlaups of variable size, with the largest events during the twentieth century occurring in 1955, 1999 and 2011. These jökulhlaups probably exceed a peak discharge of 1000 m^3 s^{-1} (Larsen *et al.*, 2013), and some destroyed or damaged bridges and roads along the south coast of Iceland.

Sources of elevation data

We used four main types of elevation data in this study, the spatial and temporal characteristics of which are summarized in Figure 2.

Optical stereo imagery: SPOT5 & Pléiades – The 13 SPOT5 stereopairs used in this study come from the SPOT5 archive produced by the French Space Agency (CNES). The dataset became publicly opened in 2021 thanks to the CNES Spot World Heritage Program, https://regards.cnes.fr/user/swh. The SPOT5 mission covered the time period from May 2002 to March 2015 and the satellite had a repeat cycle of 26 days. SPOT5 HRS images from 2007 and after were acquired as part of the SPIRIT (SPOT5 stereoscopic survey of Polar Ice: Reference Images and Topographies) project in 2007−2009 (Korona *et al.*, 2009). Pléiades satellites have been in orbit since 2011 and a total of eight stereo images were collected upon request as part of the Dinamis CNES program, https://dinamis.data-terra.org/ and the CEOS Geohazard Supersites, https://ceos.org/ourwork/workinggroups/disasters/gsnl/. The use of Pléiades stereo images for the study of glaciers is described by Berthier *et al.* (2014).

Airborne lidar – The Icelandic Meteorological Office, in collaboration with several Icelandic institutes and agencies, organised airborne lidar mapping of glaciers in Iceland in 2008–2012 (Jóhannesson *et al.*, 2013). The whole of Mýrdalsjökull was surveyed in August 2010 in three separate aerial campaigns.

ArcticDEM – The ArcticDEM digital elevation model of the Arctic was produced by NGA−NSF (National Geospatial Intelligence Agency and National Science Foundation, USA) from the stereo satellites WorldView1, 2, 3 and GeoEye-1 (Porter *et al.*, 2018). It covers all territories north of 60°N, including Iceland. Over Mýrdalsjökull, it extends from 2010 to 2018 with a total of 90 DEM segments, acquired on 41 different dates.

Aerial photographs – A series of photographs of Mýrdalsjökull from 1999 provided by Loftmyndir were processed by Belart *et al.* (2020) to produce a DEM, following the processing guidelines described by Belart *et al.* (2019).

ASTER−ArcticDEM elevation change maps – Elevation change maps based on the Advanced Spaceborne Thermal Emission and Reflection Radiometer (ASTER) and ArcticDEM data were obtained by Hugonnet *et al.* (2021) and are publicly available (https://doi.org/10.6096/13). To compare with the results of our study, maps of elevation difference for Mýrdalsjökull over 5-year periods starting in 2000 were selected and analysed.

Most images were acquired either in June−July or in September−October, corresponding to the start and end of the summer period, respectively.

Outlines and equilibrium-line altitude

Delineation of glacier and catchment outlines is an essential step in DEM analysis in order to differentiate glacier areas from ice-free terrain. Outlines of Mýrdalsjökull in 1999, 2003, 2010 and 2019 were used in this study. The 1999 outline was extracted from Belart *et al.* (2020) and the 2019 outline from Hannesdóttir *et al.* (2020). We manually delineated the 2003 and 2010 outlines on the SPOT5 orthoimage from 2003-06-20 and on a shaded relief derived from the 2010-08-09 lidar DEM, respectively. To investigate changes at a local scale, we distinguished three ice-flow catchments: a northern catchment, a southern catchment and Kötlujökull. The ice-flow catchments were defined using ice divides delineated on the 2010

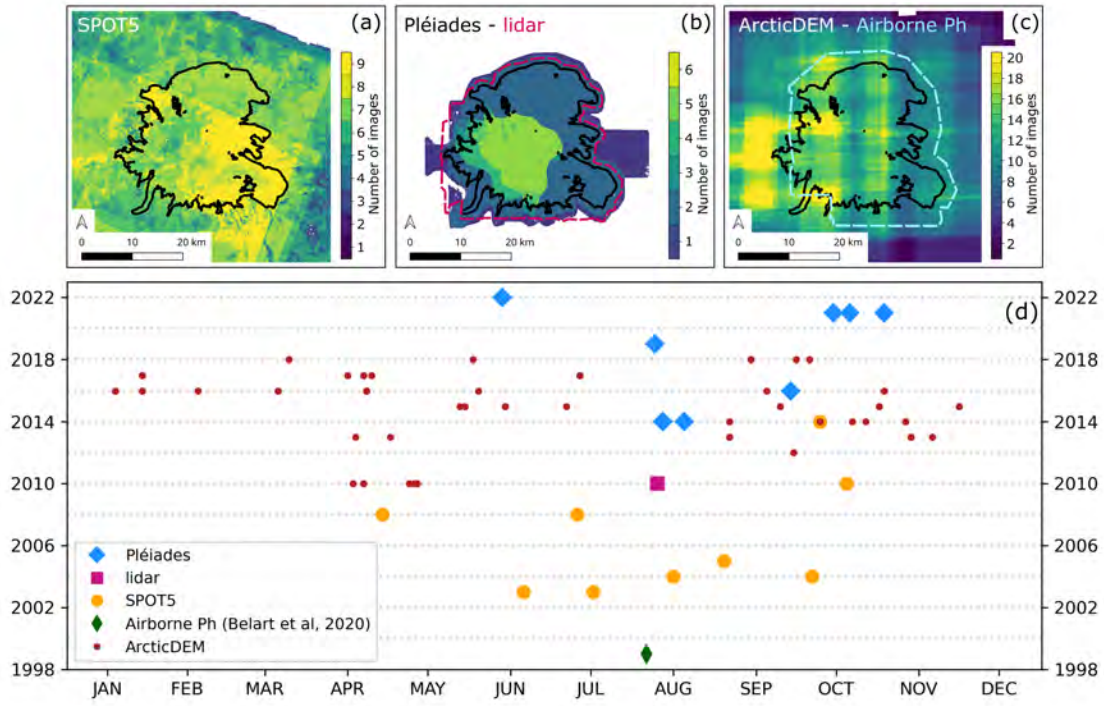

Figure 2. Spatial and temporal distribution of elevation data. Spatial extent of the studied scenes presented as the number of observations per pixel or as the outline of the scene. (a), (b) and (c) show the number of SPOT5 DEMs, Pléiades DEMs and ArcticDEM DEMs, respectively. The extent of the lidar DEM is indicated as a dashed line on (b) and the extent of the 1999 photogrammetric DEM from Belart *et al.* (2020) is shown as a dashed line on (c). The temporal distribution of all datasets is presented on (d). – *Dreifing hæðargagna í tíma og rúmi. Landfræðileg dreifing er sýnd sem fjöldi hæðarmælinga í hverjum punkti eða með útlínu viðkomandi gagna. (a), (b) og (c) sýna fjölda mælinga á grundvelli SPOT5, Pléiades og ArcticDEM landlíkana. Útlína landlíkana sem byggja á leysimælingu úr flugvél er sýnd með slitnum ferli á (b) og útlína landlíkans sem unnið var með myndgreiningu loftmynda frá 1999 er sýnt með slitnum ferli á (c). Dreifing gagnanna í tíma er sýnd á (d).*

lidar DEM and assumed not to vary with time. The 1999 and 2019 glacier outlines and the extents of the glacierized catchments are shown in Figure 1b.

The equilibrium-line altitude (ELA), defined as the elevation of the line separating the ablation area and the accumulation area, comes from Belart *et al.* (2020). It was obtained using the snowline at the end of the summer season as a proxy, based on a SPOT5 orthoimage from October 5th 2004.

METHODS

DEM generation – First, DEMs were created from the raw satellite stereo images (SPOT5, Pléiades) and from the lidar point clouds, using the Ames Stereo Pipeline (ASP) software (Beyer *et al.*, 2018). The lidar point clouds from 2010 were interpolated using ASP's routine *point2dem*, into 2×2 m DEMs that were then mosaicked into a single DEM using the routine *dem_mosaic*.

The Pléiades stereo images were processed using the ASP tools, using the routines and set of parameters indicated in Shean *et al.* (2021). The SPOT5 stereo images were processed in a similar manner to the Pléiades images, with the addition of the pre-processing routine *add_spot_rpc*. To obtain a consistent dataset, all DEMs were resampled to a 10×10 m pixel size.

DEM co-registration – Prior to volume and mass calculations, potential biases in the DEMs have to be cor-

rected. Using uncorrected DEMs can lead to inaccurate estimates of glacier changes. These biases can be horizontal, vertical, planar tilt, or non-linear (e.g., jittering) (Girod *et al.*, 2017; Dehecq *et al.*, 2020; Hugonnet *et al.*, 2022). Therefore, the first step in the analysis consists of co-registering each DEM to a common reference DEM. Nuth and Kääb (2011) propose a robust co-registration method based on elevation difference and slope and aspect on stable terrain surrounding the glacierized area. An automated and iterative implementation of this algorithm is available on the github repository *demcoreg* (Shean *et al.*, 2016), https://doi.org/10.5281/zenodo.5733347. We used the IslandsDEM, a seamless and bias-corrected mosaic from ArcticDEM (Porter *et al.*, 2018) and lidar (Jóhannesson *et al.*, 2013) from the National Land Survey of Iceland, https://dem.lmi.is as the reference DEM as it offers complete coverage of a large area on and around the glacier. The co-registration was applied to all DEMs derived from Pléiades, SPOT5 and ArcticDEM.

Filtering – Depending on the imagery and sensor characteristics, various artefacts can appear in the DEMs. Outliers can be caused by clouds, saturation in snow or dark areas, or errors at specific scan lines in the case of the SPOT5 data. Therefore, two filtering methods were combined and applied to all DEMs generated from SPOT5 and ArcticDEM datasets as well as the 1999 DEM from aerial photographs.

Following Hugonnet *et al.* (2021), we applied a spatial filter based on a comparison between the DEM to be filtered and the mosaicked lidar DEM used as a reference DEM. For each pixel, the maximum h_{max} and minimum h_{min} elevation of the reference DEM within a r radius area of 10 m were calculated. Then, all pixels where the elevation is higher than $h_{max} + dh_{thresh}$ or lower than $h_{min} - dh_{thresh}$ were masked, with an elevation threshold dh_{thresh} of 50 m.

Based on the statistical characteristics of the dataset composed of all DEMs used in this study (i.e. 1999 airborne DEM, SPOT5, Pléiades, lidar and ArcticDEM) we performed a median-NMAD filtering. The normalized median absolute deviation (NMAD) is a metric to evaluate data dispersion. It is less sensitive to outliers than the standard deviation and thus widely used to estimate DEM vertical precision (Hohle *et al.*, 2009). The NMAD is computed as follows:

$$NMAD = 1.4826 \cdot \mathrm{median}(|h_j - m_h|)$$

where h_j is the elevation of pixel j and m_h is the median of all considered elevations. For each 10×10 m pixel, a median and NMAD value of all available elevations were calculated from the DEM dataset to obtain the corresponding mosaics. Then, we used a multiplier K, adjusted to 10 in this study, so that for each DEM analysed, a pixel would be considered an outlier and eliminated from the respective DEM if its elevation was outside the interval $\mathrm{median} \pm (K * NMAD)$.

Void interpolation – Most of the DEMs used in this study contain data gaps, mainly due to clouds, filtering or partial coverage of the initial stereo images. The amount of gaps also depends on the nature of the sensor. For example, SPOT5 DEMs, often noisy, have much much more voids than Pléiades or lidar DEMs. Since complete elevation difference maps (dh maps) are required to calculate volume and mass changes, a void interpolation step is necessary. Following McNabb *et al.* (2019), we first applied a spatial interpolation with a maximum search distance of 100 m to preserve gradual and continuous changes as much as possible around the gaps. Then, we used a local hypsometric interpolation based on the entire ice cap to fill the larger remaining voids.%vspace0.3em

Pairwise co-registration – Independently of the GP regression (see below), we also created dh maps from pairs of DEMs. A total of eight DEM pairs were highlighted as they fulfilled the two following criteria: acquired at least two years apart (in order to get a sufficiently large signal of volume change), and at the same time of year (<1 month difference). Although all DEMs were co-registered to a reference DEM, some residual shifts could still remain and hamper the analysis of the dh maps. A pairwise co-registration was therefore performed for each DEM pair studied, considering the older DEM as the reference DEM. The amplitude of the horizontal and vertical remaining shifts was systematically less than 1 m, i.e. one order of magnitude lower than the shifts found in the first co-registration.

Gaussian Process regression – To compute volume change and geodetic mass balance, dh maps from DEMs of exact timestamps are commonly used. However, this method has some limitations. In particular, two DEMs acquired more than a few weeks apart require a correction for their dh map to show elevation and volume changes that are not affected by seasonal signals. DEMs can be seasonally corrected individually using surface mass-balance models forced with climatic records as in Belart *et al.* (2019, 2020). However, this process is time-consuming and complicated to use when considering a large number of DEMs. Consequently, alternative numerical methods have been developed to overcome these problems and obtain temporally continuous datasets from scattered observations in time. Considering all DEMs as a time stack, a temporal regression can be computed for each pixel to produce a gapless time series of elevation maps. Then, volume and mass-balance estimates can be calculated in precise time windows, which is convenient for glaciological analysis. Hugonnet *et al.* (2021) introduced Gaussian Process (GP) regression to temporal glacier-elevation analysis, a state-of-the-art regression approach that is based on modelling of the temporal covariance of glacier elevations. This method is implemented in the Python package *pyddem* (https://pypi.org/project/pyddem/). Using the covariance parameters optimized on 20 years of global glacier elevation data (Hugonnet *et al.*, 2021), we ran the Gaussian Process regression on a time stack of 134 non-mosaicked DEMs. These DEMs, co-registered to the IslandsDEM, are composed of 116 ArcticDEM DEMs, 9 SPOT5 DEMs, 8 Pléiades DEMs and 1 airborne photogrammetric DEM. The lidar DEM was intentionally not included in the stack for later validation of the GP results. Due to computing limitations, the GP was run at a maximum spatial resolution of 15×15 m and a 30-day time step during the period $1999-2021$. As a result, we obtained a monthly time series with 264 time steps of interpolated elevation.

Mass-balance computation

Volume change and mass balance – In order to investigate glacier changes over time, several indicators can be computed. First, using complete dh maps, we calculated the total volume change during the corresponding period as $\Delta V = \overline{\Delta h} \cdot A_{ini}$, where $\overline{\Delta h}$ (m) is the mean elevation change and A_{ini} (m^2) the area of the glacier (in this case the spatial union of the glacier extent at the two points in time). For the years 1999, 2003, 2010 and 2019, the area was directly extracted from the outline. For other years, a linear interpolation of the area was computed based on those four values. To be consistent with glaciological conventions, hydrological years, defined as October 1$^{\text{st}}$ to September 30$^{\text{th}}$, were taken as a reference period in all further calculations.

The geodetic mass-balance rate $\dot{B}$ (m w.e. a^{-1}) over the observation period Δt was obtained as follows:

$$\dot{B} = \frac{\Delta V \cdot f_{\Delta V}}{\overline{A} \cdot \Delta t}$$

where $f_{\Delta V}$ (kg m^{-3}) is the conversion factor from volume to mass change and $\overline{A} = \frac{1}{2} \cdot (A_{ini} + A_{end})$ is the average area during the observation period. Following Huss (2013), $f_{\Delta V}$ was set to 850 ± 60 kg m^{-3}. However, it is crucial to note that this value cannot be used with high confidence for short periods (<4 years) because of potentially significant changes in snow density from one year to another (Huss, 2013).

In order to study the local variability of mass balance, we defined three subregions of the ice cap (Figure 1b). As the northern and southern outlets are exposed to different climatic regimes, two corresponding areas were delineated: Sléttjökull and Öldufellsjökull outlets were included in the northern catchment; Goðalandsjökull and Sólheimajökull outlets were encompassed in the southern one. Kötlujökull was defined as a separate area. Mass balance was calculated on the three catchments using the same methodology as for the entire ice cap. We computed the mass balance for periods of one and five hydrological years between 1999 and 2019. For simplicity, the uncertainties calculated on the stable terrain around Mýrdalsjökull were used for the catchments' mass-balance estimates.

Uncertainty – We used the method developed by Hugonnet *et al.* (2022) to determine the uncertainty in mean elevation difference $\sigma_{\overline{\Delta h}}$. This approach takes into account two statistical effects that are often not considered in elevation error estimates.

DEMs present significant heteroscedasticity, i.e. there is a precision variability in the elevation observations. To obtain an estimate of the elevation uncertainty, we modelled the heteroscedasticity using two explanatory variables: the terrain slope and curvature.

Elevation errors are spatially correlated (e.g., Rolstad *et al.*, 2009; Magnússon *et al.*, 2016). In other words, the elevation errors of two neighboring pixels cannot be considered independent. This spatial correlation can occur over different ranges: a short-range (related to the DEM resolution) and a long-range (linked to instrument noise and imperfections). We used robust variograms estimation and modelling to describe these spatial correlations in our elevation-uncertainty analysis (Figure 3), with the tools implemented in the Python package xDEM (https://doi.org/10.5281/zenodo.4809698).

The uncertainty in volume change was estimated assuming that the uncertainties in glacier area and mean-elevation difference were not correlated:

$$\sigma_{\Delta V}^2 = (\overline{\Delta h} \cdot \sigma_{\overline{A}})^2 + (\overline{A} \cdot \sigma_{\overline{\Delta h}})^2$$

Then, the uncertainty σ_m in the geodetic mass balance was derived, assuming uncorrelated error sources from density conversion, glacier area and volume change:

$$\sigma_m^2 = (\frac{\partial \dot{B}}{\partial \Delta V} \cdot \sigma_{\Delta V})^2 + (\frac{\partial \dot{B}}{\partial f_{\Delta V}} \cdot \sigma_{f_{\Delta V}})^2 + (\frac{\partial \dot{B}}{\partial \overline{A}} \cdot \sigma_{\overline{A}})^2$$

where $\sigma_{f_{\Delta V}} = 60$ kg m^{-3} is the conversion factor uncertainty and $\sigma_{\overline{A}}$ is the area uncertainty calculated as 2% for the average area $\overline{A}$. This area uncertainty is somewhat lower than the 5% area uncertainty used by Raup *et al.* (2014) and Hugonnet *et al.* (2021) due to the large size of Mýrdalsjökull ice cap and its approximately circular shape, which may be assumed to lead to a comparatively low value for the relative area uncertainty. The variations in the area of Mýrdalsjökull in the past two decades also show an internal agreement between years that indicates a relative accuracy substantially better than 5% (Hannesdóttir *et al.*, 2020). The overall uncertainty of the mass balance is insensitive to the value chosen for the area uncertainty so the choice of 2% rather than 5% for the area uncertainty has negligible impact on our results.

RESULTS

Elevation time series

As a result of the GP regression, a time series of elevation with a time step of 30 days was generated for each 15×15 m pixel of Mýrdalsjökull. To illustrate the variety of patterns that are captured by the GP regression, we selected three pixels from diverse locations: one from the accumulation area, one from the ablation area and one from a cauldron (Figure 4). The characteristics of the elevation variations in the period 1999−2021 differ greatly depending on the location. Differences in the amplitude of the seasonal signal are also noticeable. The elevation time series from the accumulation area is steady over the two decades, slightly decreasing from 1999 to 2012 and then gently increasing until 2016 before leveling off. The seasonal variation, around ∼5 m, is quite large. In the ablation area, the expected lowering of the elevation is remarkably clear, reaching almost 50 m in 20 years (Figure 5) with an attenuated seasonal signal. Last, the elevation time series at the cauldron is erratic: periods of thickening and thinning alternate with no clearly identified frequency. The seasonal variation is substantial. In all three locations, the non-uniform temporal distribution of DEMs leads to substantial differences in the dh uncertainty values. The 2-sigma interval is smaller as the number of data available is larger.

Validation and evaluation

Comparison with the lidar DEM – We performed a comparison between the lidar DEM from 2010-08-09 and the closest GP-interpolated DEM (2010-08-01). We found a NMAD of elevation differences of 3.33 m. Using the co-registration tools without masking the glacier, a shift of +1.66 m (x), +6.74 m (y) and +0.58 m (z) between the two DEMs was obtained. These results are comparable to the shifts obtained with the pairwise co-registration.

Comparison on survey dates – First, mass-balance values $\dot{B}_{dh\ map}$ were calculated using the eight dh maps previously selected (see Section 3.1). The corresponding mass-balance ranges between -0.27 ± 0.01 m w.e. a^{-1} (2010-10-19 to 2014-10-09) and

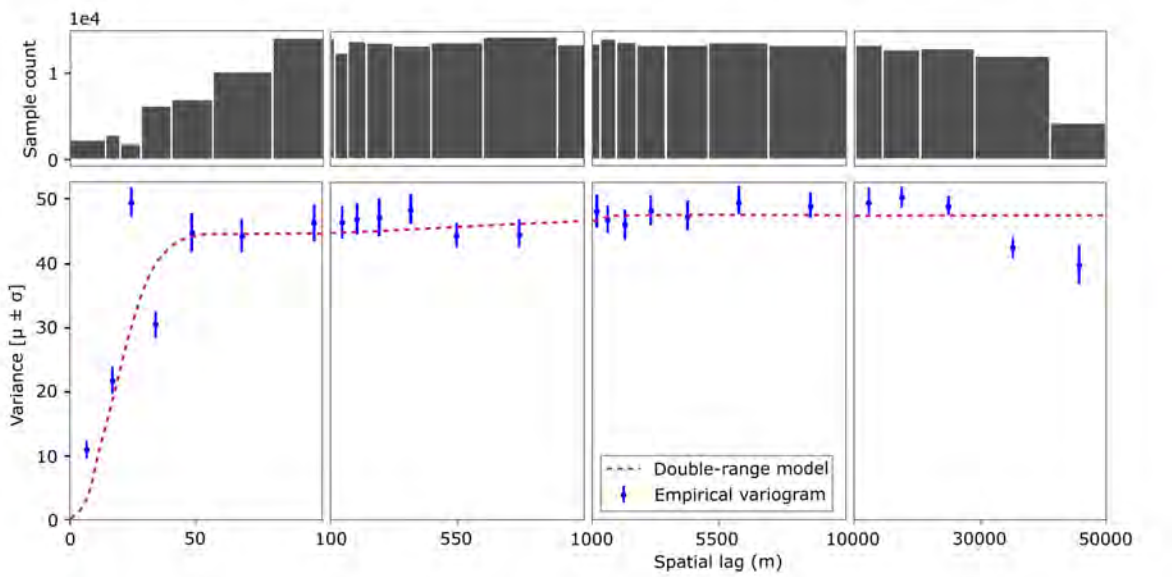

Figure 3. Variogram obtained on stable terrain from the dh map between 2003-07-16 and 2008-07-09 SPOT5 DEMs using xDEM. A short-range correlation (up to ∼100 m) and a long-range correlation (from ∼1000 m) can be identified. The double-range spherical function used to model the variogram accounts for both correlation ranges. The sample count shows the amount of measurement pairs used to compute each value of the variogram. – *Tölfræðileg dreifing hæðarmismunar á jökullausu landi milli SPOT5 landlíkana frá 2003-07-16 og 2008-07-09 reiknuð með xDEM. Sjá má mismunandi mikla fylgni yfir stuttar (allt að ∼100 m) og langar (lengri en ∼1000 m) vegalengdir. Sívalningssamhverft fall sem notað er til þess að lýsa breytingu fylgninnar með fjarlægð tekur tillit til þessa mismunar. Súlurit sýnir punktafjölda sem notaður er til þess að meta hvert fylgnigildi í dreififallinu.*

-2.82 ± 0.12 m w.e. a^{-1} (2008-07-09 to 2010-08-09), with a large decrease in 2010 followed by less negative values during the past decade.

Secondly, the geodetic mass balance was also estimated using the GP-interpolated DEMs ($\dot{B}_{GP}$). In order to evaluate the results obtained with the Gaussian Process regression, a comparison with the original dh maps was performed. For each survey date, the temporally closest GP-interpolated DEM was extracted to compute the GP dh map equivalent to the map directly derived from the original DEMs. Mass balance using both methods was compared for the eight different periods (Figure 6).

Overall, the GP-interpolated DEMs lead to similar mass-balance values to those from the original DEMs. The GP and original estimates overlap within 2-sigma uncertainties except in two cases (October 2004 to October 2010 and August 2010 to August 2014). It should be noted that when the original dh map includes at least one Pléiades or lidar DEM, the two estimates show good agreement. For example, the $\dot{B}_{dh\ map}$ between 2008-07-09 SPOT5 DEM and 2010-08-09 lidar DEM is -2.82 ± 0.12 m w.e. a^{-1}, compared to the $\dot{B}_{GP}$ of -2.68 ± 0.20 m w.e. a^{-1} computed between 2008-07-01 and 2010-08-01. However, when two SPOT5 DEMs or one SPOT5 DEM and the airborne photogrammetry DEM are involved, the agreement is worse. First, the $\dot{B}_{dh\ map}$ uncertainties are larger than those of $\dot{B}_{GP}$. Then, $\dot{B}_{GP}$ overlap only at the extremity of the uncertainty bar, with both less negative (August 1999 to July 2003, July 2003 to July 2008, October 2004 to October 2010) and more negative (October 2010 to October 2014) values than $\dot{B}_{dh\ map}$.

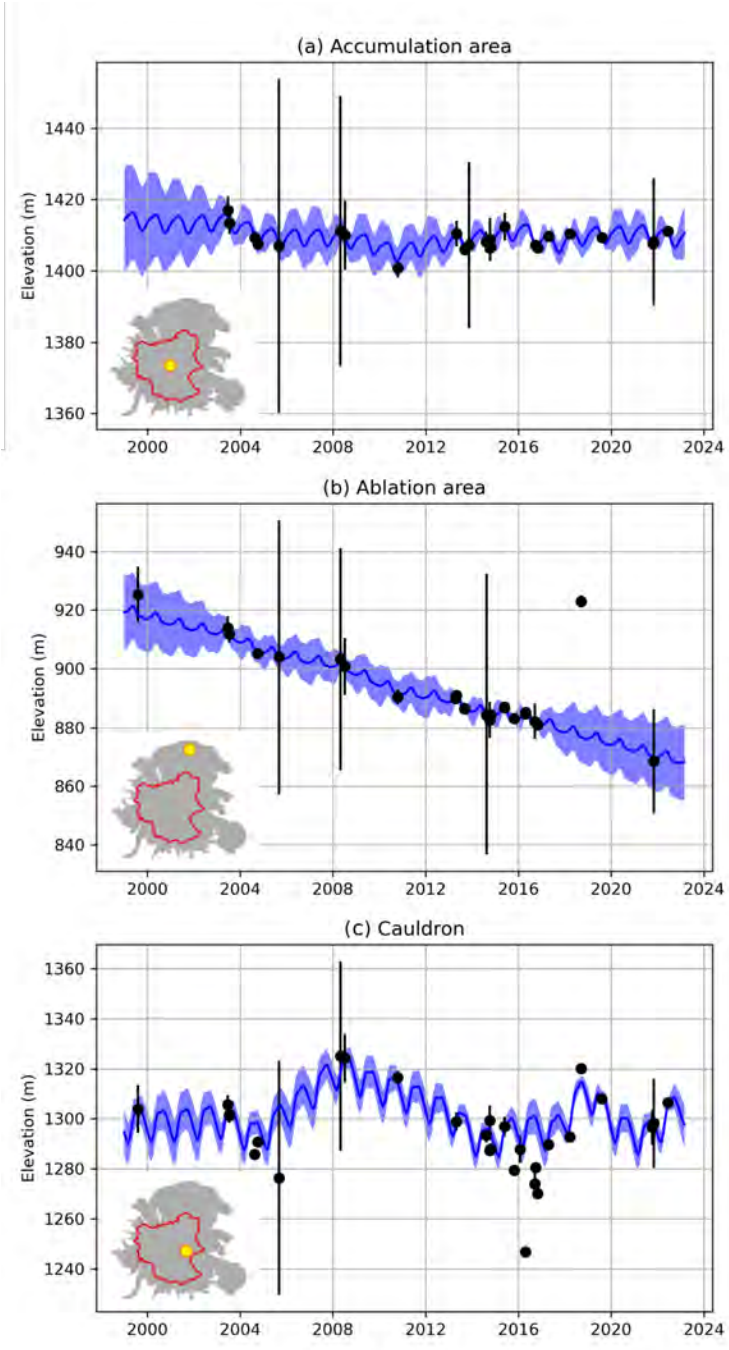

Figure 4. Elevation time series obtained from GP regression for pixels from different locations on Mýrdalsjökull. (a) Accumulation area, (b) Ablation area, (c) Cauldron. The blue line corresponds to the GP regression time series. The associated $1\,\sigma$ interval is indicated with a blue envelope. Elevations extracted from preprocessed DEMs and their $2\,\sigma$ uncertainty are shown as black dots and vertical lines.– *Tímaraðir GP-brúaðrar yfirborðshæðar á nokkrum stöðum á Mýrdalsjökli. (a) Staður á ákomusvæði, (b) á leysingarsvæði, (c) í jarðhitakatli.* $1\,\sigma$ *óvissubil er sýnt með blárri skyggingu. Hæð skv. landlíkönum og* $2\,\sigma$ *óvissubil er sýnd með svörtum punktum og lóðréttum línum.*

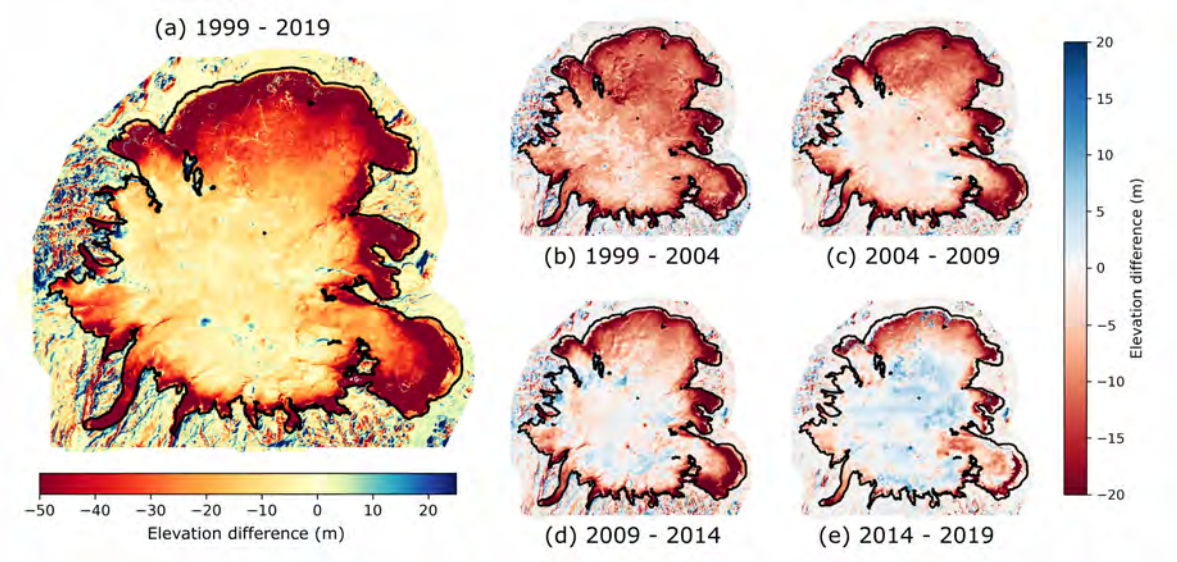

Figure 5. Elevation difference maps computed with GP-interpolated DEMs. Elevation differences (a) over the entire period 1999−2019 and (b), (c), (d), (e) on periods of 5 hydrological years (October 1st to September 30th) starting in 1999. The 1999 outline is shown in black. – *Hæðarmunur reiknaður með GP-brúuðum landlíkönum. (a) Allt tímabilið 1999−2019. (b), (c), (d), (e) Fimm vatnsára tímabil (1. okt. til 30. sept.) frá 1999. Jökuljaðarinn árið 1999 er sýndur með svörtum lit.*

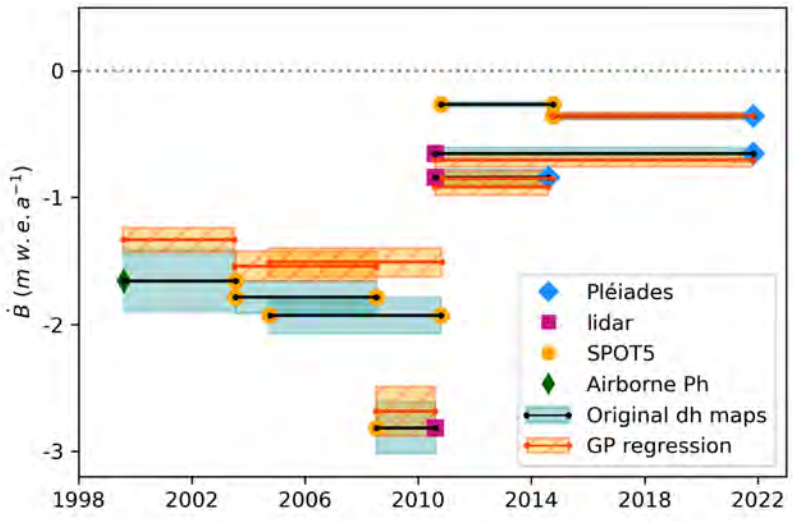

Figure 6. GP-based mass-balance evaluation. Mass balance computed on survey dates (eight original *dh* maps). Values and 2-sigma uncertainties obtained with the original elevation difference maps are shown in blue and GP results in orange. – *Landlíkanafkoma reiknuð milli mælidaga (blár litur) (átta landlikön) og með tölfræðilegri GP-brúun (appelsínugulur litur). 2σ óvissa er sýnd með skyggingu.*

Those discrepancies might be explained by the higher level of noise of the SPOT5 and airborne photogrammetric DEMs and the general smoothing of the GP regression. It is interesting that the mass balance computed from the GP-interpolated DEMs is systematically less negative than the mass balance derived from the original DEMs for the entire period 1999–2010 by ca. 0.2–0.5 m w.e. a^{-1}.

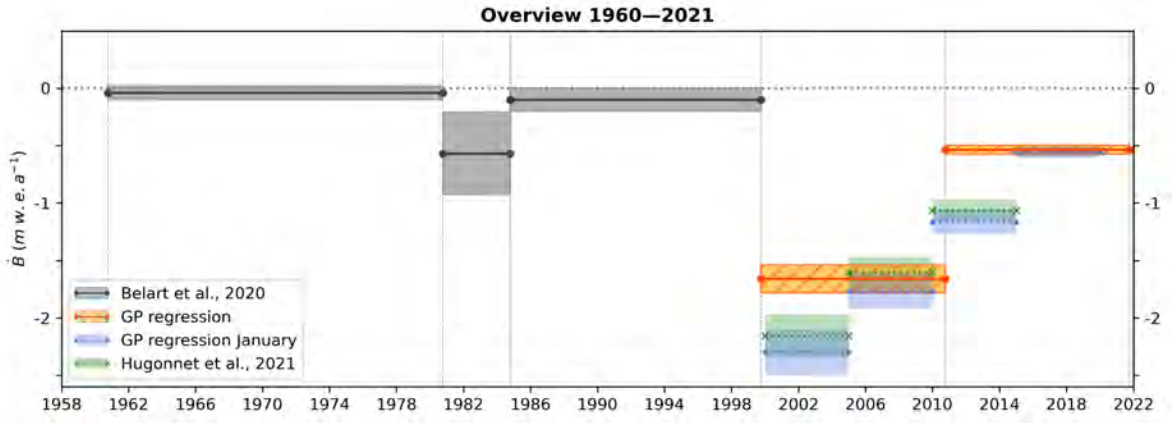

Figure 7. Mass balance overview from 1960 to 2021. Previous results from Belart *et al.* (2020) are shown in grey, GP mass balance on 11-hydrological-year periods are indicated in orange with a 2-sigma uncertainty. Comparison between mass balance obtained with the elevation-change maps from Hugonnet *et al.* (2021) (green) and GP results of this study (blue). For consistency with the results of Hugonnet *et al.* (2021), this comparison was done using this study's GP DEMs created from January 1st to December 31st for 5-year periods starting in 2000. – *Yfirlit um afkomu Mýrdalsjökuls á tímabilinu 1960 til 2021. Fyrri niðurstöður Belarts o.fl. (2020) eru sýndar með gráum lit og niðurstöður tölfræðilegrar GP-brúunar yfir 11 vatnsára tímabil með appelsínugulum lit. 2σ óvissubil er sýnt með skyggingu. Einnig er sýndur samanburður á niðurstöðum Hugonnet o.fl. (2021) (grænn litur) og niðurstöðum þessarar greinar (blár litur). Til samræmis er landlíkanafkoman reiknuð yfir fimm almanaksár með upphafi árið 2000 í þeim samanburði.*

Table 1. Mass balance from 1960 to 2021 on Mýrdalsjökull and on three catchment areas. – *Landlíkanafkoma Mýrdalsjökuls í heild og þriggja ísflæðisviða á tímabilinu 1960 til 2021.*

Period	**Mýrdalsjökull** $\dot{\mathbf{B}}$ (m w.e. a^{-1})	**Northern catchment** $\dot{\mathbf{B}}_{\mathbf{N}}$ (m w.e. a^{-1})	**Southern catchment** $\dot{\mathbf{B}}_{\mathbf{S}}$ (m w.e. a^{-1})	**Kötlujökull** $\dot{\mathbf{B}}_{\mathbf{k}}$ (m w.e. a^{-1})
1960−1980	-0.04 ± 0.06			
1980−1984	-0.57 ± 0.36			
1984−1999	-0.10 ± 0.10			
1999−2005	-1.83 ± 0.13	-2.22 ± 0.13	-1.52 ± 0.13	-1.64 ± 0.13
2005−2010	-1.45 ± 0.11	-1.93 ± 0.11	-1.24 ± 0.11	-1.21 ± 0.11
2010−2016	-0.64 ± 0.05	-0.90 ± 0.05	-0.42 ± 0.05	-0.71 ± 0.05
2016−2021	-0.41 ± 0.03	-0.57 ± 0.03	-0.24 ± 0.03	-0.40 ± 0.03

Geodetic mass-balance

Ice cap mass balance – The mass balance from 1960 to 2021 based on results from this study and from Belart *et al.* (2019) are presented on Figure 7.

Catchment scale analysis – The observed general variations of the mass balance are the same for the three catchments areas as for Mýrdalsjökull ice cap as a whole (Table 1, Figure 8a). During the past two decades, mass balance becomes slowly less negative and almost reaches positive values over the period 2014−2019. The last period is affected by the years 2014 and 2015 being exceptionally wet and cold (e.g., Aðalgeirsdóttir *et al.* 2020), which explains the near-zero observed mass balance.

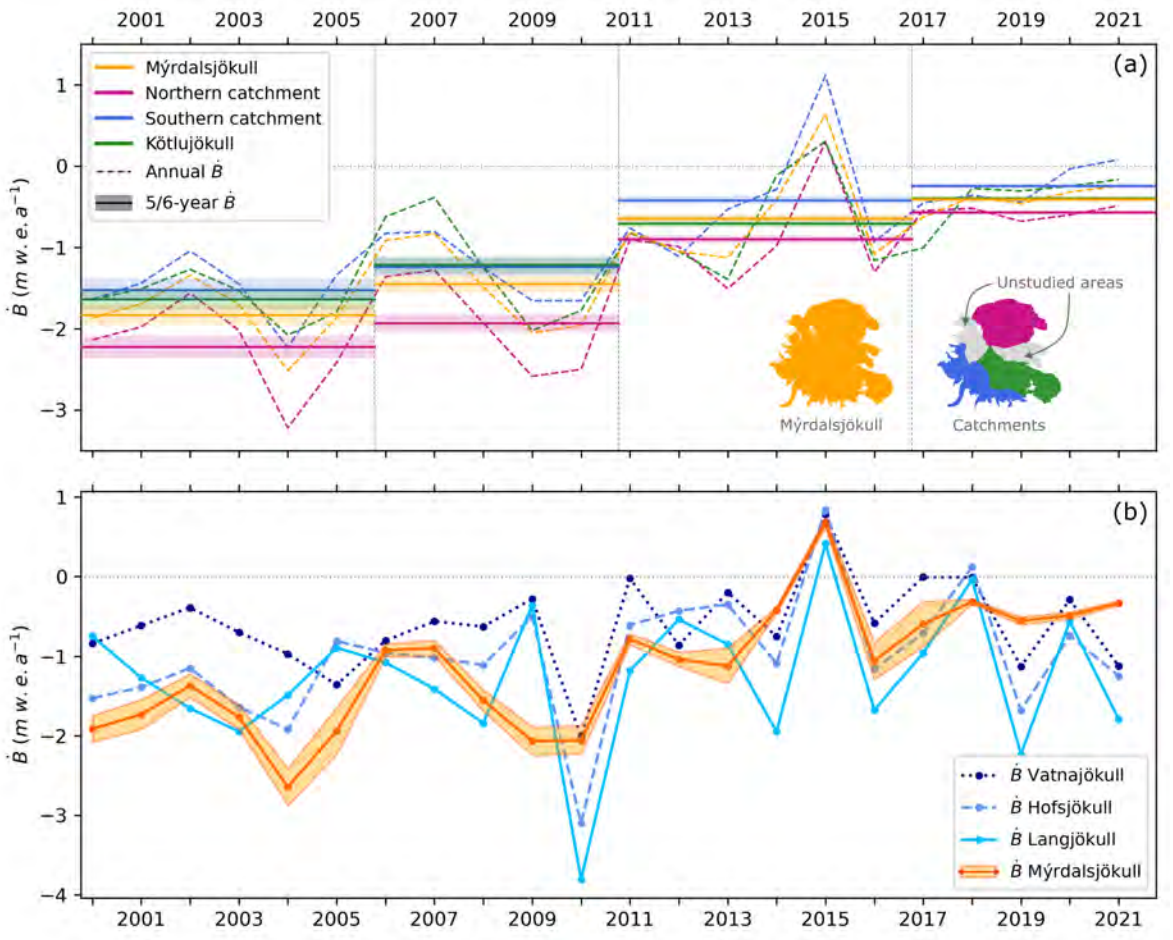

Figure 8. Mass-balance comparisons. (a) Mass balance of ice-flow catchments obtained from the GP-interpolated elevation dataset. Dashed lines represent annual mass balance computed on hydrological years. 5- or 6-hydrological-year mass balance and the corresponding 2-sigma uncertainties are indicated with horizontal solid lines with shaded bars. (b) Comparison between glaciological mass balance (surface and non-surface mass balance) of the three largest Icelandic ice caps and geodetic annual mass balance of Mýrdalsjökull. – *Afkomusamanburður. (a) Afkoma ísflæðisviða á Mýrdalsjökli reiknuð með tölfræðilegri GP-brúun. Slitnar línur sýna afkomu vatnsára (1. okt. til 30. sept.). Afkoma 5 og 6 ára tímabila með 2σ óvissu er sýnd með heildregnum línum og skyggðum borðum. (b) Samanburður á jöklafræðilegri afkomu þriggja stærstu jöklanna, sem leiðrétt hefur verið fyrir innri leysingu og leysingu við botn, og landlíkanafkomu Mýrdalsjökuls.*

The trend after 2017 is in line with other glaciers, Vatnajökull, Langjökull and Hofsjökull, based on their records of glaciological measurements (Pálsson *et al.*, 2022a, 2022b; https://icelandicglaciers.is).

The northern catchment has the most negative mass balance and the southern catchment the least negative mass balance. Kötlujökull and the entirety of Mýrdalsjökull have similar mass-balance values that differ at most by 0.31 m w.e. a^{-1}.

Despite climatic contrasts between the northern and southern catchments of Mýrdalsjökull, no significant differences in terms of temporal variability appear between the catchments (Figure 8). Exposed to a more inland and less fluctuating climate, the northern catchment could have been expected to experience less temporal variability than the southern catchment (Hock *et al.*, 2009). This was not the case, at least not for the 20-year period studied here.

DISCUSSION

Analysis of multitemporal DEMs

Hugonnet *et al.* (2021) introduced a new method in multi-temporal DEM processing that improves some aspects of DEM analysis and geodetic mass-balance computations. It can be used through automated commands with tools implemented in the Python package *pyddem*.

Pyddem solves the problem with incomplete spatial and temporal coverage common in geodetic mass-balance studies (e.g., Fischer *et al.*, 2015; Andreassen *et al.*, 2016) caused by multiple factors such as cloud cover, sensor characteristics and data accessibility. GP produces a temporally and spatially continuous elevation dataset which enables internally consistent mass-balance computations over precise areas and time periods.

Another advantage of this method is its robustness. The GP regression has been validated through a comparison between ICESat data using DEMs generated from ASTER or retrieved from the ArcticDEM archive (Hugonnet *et al.*, 2021). In our study, the comparison between a GP-interpolated DEM and the lidar DEM also shows good agreement.

The data filtering included in the GP implementation in *pyddem* leads to much smoother maps and lower uncertainties in subsequent calculations (Figures 5 and 7). The method, initially designed for processing ASTER and Arctic DEM data as part of a global analysis of glacier mass loss includes efficient steps of filtering and weighting. Our study shows that other data, such as Pléiades- and SPOT5-based DEMs, can be added as part of the temporal DEM stack.

Although it provides substantial improvements in DEM treatment, the GP method has some limitations. First, the GP regression does not fully capture annual and seasonal trends. This is shown from the elevation time series extracted at specific locations on the glacier from Figure 4, as the $1-\sigma$ interval remains large around seasonal variations.

Furthermore, the GP regression produces a general smoothing of elevation changes, especially when data are missing. For example, the elevation drop in 2010 related to the Eyjafjallajökull eruption is accurately reproduced (Figure 8). However, the Gaussian Process analysis extrapolates the low mass balance observed in 2010 to the year 2009 as no DEM from that year is available to constrain the GP regression (cf. the temporal distribution depicted in Figure 2d). Such a negative mass balance is not expected for 2009 as no particular climatic or volcanic event was observed in that year.

An adaptation of the kernels used in the GP could have been considered to better account for the conditions of Mýrdalsjökull. For example, the model of temporal covariance could be changed to more accurately take into account the exceptional melting in summer 2010 following the Eyjafjallajökull eruption. However a more sensitive kernel could also affect and overfit the beginning and end of the elevation time series where data are scarce.

Mass balance

To obtain a longer perspective of mass balance over the past decades, estimates for the period $1960-1999$ were extracted from (Belart *et al.* (2020) (Figure 7, Table 1). During the second half of the twentieth century, $\dot{B}$ was rather stable and close to $0\,\mathrm{m}$ w.e. a^{-1}. Then, the annual mass balance dropped in the late 1990s or early 2000s to $-1.82 \pm 0.16\,\mathrm{m}$ w.e. a^{-1} before becoming gradually less negative.

Comparison with Hugonnet et al. (2021)

We performed another comparison with the mass balance $\dot{B}_{Hug}$ computed with the elevation change maps from Hugonnet *et al.* (2021). These were obtained by applying the same GP method to ASTER and ArcticDEM elevation datasets. As elevation data were only available for January 1^{st} to December 31^{st}, we

adapted the $\dot{B}_{GP_{Jan}}$ calculation to this period for consistency (see Figure 7). Mass balance from that study tends to be less negative than those obtained here. Nevertheless, our study shows overall agreement with Hugonnet *et al.* (2021).

Annual mass balance and conversion factor

Annual mass-balance values were computed in this study. They are useful to derive a temporally detailed dataset, for example to compare with *in situ* observations (Figure 8b) and climatological data. Nevertheless, the limited amount of data leads to large uncertainties, and it is not possible to calculate precise annual mass-balance values. (Huss, 2013) investigated the robustness of the conversion factor $f_{\Delta V}$. As the firn density profile continually evolves with accumulation and melting events, the assumption of a constant value for density conversion inescapably leads to large uncertainties, especially for short periods (<4 years).

Although the density conversion factor may be expected to vary for short time periods, estimating annual mass balance from a continuous time series still helps to identify short-term variations and patterns. For longer study periods, trends become more robust at the cost of smoothing short-term variability. In addition, there are several ways to address the limitations of the conversion-factor estimate. One possibility is to adapt density conversion uncertainties for short periods. Another possibility is to use *in situ* density measurement (Ágústsson *et al.*, 2013) to adapt the conversion factor $f_{\Delta V}$.

Comparison with glaciological mass balance from other Icelandic ice caps

Mean specific surface mass-balance records were extracted from Aðalgeirsdóttir *et al.* (2020) for the three largest Icelandic ice caps. Winter and summer mass balance has been measured in *in situ* surveys every year since 1991/92, 1987/88, 1996/97 for Vatnajökull (∼60 locations), Hofsjökull (∼25 locations) and Langjökull (∼25 locations), respectively. The annual specific surface mass balance derived from those datasets was corrected following Jóhannesson *et al.* (2020) to include the non-surface mass-balance components (internal and basal melting and calving).

Figure 8b shows the annual geodetic mass balance of Mýrdalsjökull (from GP-based DEMs) and the corrected glaciological mass balance (based on the *in situ* observations) of Vatnajökull, Hofsjökull and Langjökull (Aðalgeirsdóttir *et al.*, 2020; Thorsteinsson *et al.*, 2017; Pálsson *et al.*, 2021a,b). The general mass-balance trend is similar for all four glaciers. First, there is a gradual decrease in mass loss during one and a half decades starting in the late 1990s and early 2000s. This tendency comes to an end in 2015, when the mass balance reaches a positive value. After 2015, an increasing trend of mass loss is observed until the end of the records. Over the study period, the annual geodetic mass balance of Mýrdalsjökull fluctuates from -2.64 to $+0.68$ m w.e. a^{-1}. It varies over the same range as for the other ice caps, for which the mass-balance rate varies from -2.01 to $+0.78$ m w.e. a^{-1} for Vatnajökull, from -3.10 to $+0.84$ m w.e. a^{-1} for Hofsjökull and –3.80 to $+0.41$ m w.e. a^{-1} for Langjökull.

The four ice caps are generally similar in terms of temporal variability. One-time events induce comparable fluctuations in the mass balance of them all. The Eyjafjallajökull eruption in 2010 leads to extremely negative mass balance for Vatnajökull (-2.01 m w.e. a^{-1}), Hofsjökull (-3.10 m w.e. a^{-1}) and Langjökull (-3.80 m w.e. a^{-1}). This effect is also clearly visible on Mýrdalsjökull in 2010 (-2.06 m w.e. a^{-1}) although the strongly negative value leaks into the year 2009 (-2.07 m w.e. a^{-1}), as previously mentioned, due to the lack of data to constrain the GP regression. Likewise, the four ice caps all have positive annual mass balance in 2014−2015 related to a climatic anomaly, also observed by Aðalgeirsdóttir *et al.* (2020) and Noël *et al.* (2022).

Mass balance for ice-flow catchments

Because of climatic disparities between the northern and southern outlets of Mýrdalsjökull, differences in mass-balance variability can be expected. As the south area receives a large amount of precipitation, it could be more sensitive to snowfall and rainfall fluctuations and therefore show more variation with time (Björnsson and Pálsson, 2008; Crochet (2007). This was observed by Belart *et al.* (2020) when comparing mass-balance rates between decades for the

small glaciers and ice caps in Iceland. The southern catchment of Mýrdalsjökull showed significant mass gain between 1960 and 1984 followed by a strong retreat from 1984 to 2010. Conversely, northern outlets experienced an overall declining trend over the five decades. However, in our study, focusing on a short time period of two decades, larger variability is not observed in the southern catchment (Figure 5). In the past two decades, the northern and southern halves of Mýrdalsjökull have shown similar mass-balance variations since 2000. The variability related to climate of South Mýrdalsjökull may require a longer study period to be observed. In other words, longer periods of climate variation could be needed to detect different statistical characteristics of the southern and northern ice-flow basins.

CONCLUSIONS

This study presents geodetic mass-balance estimates for the Mýrdalsjökull ice cap over the past two decades, 1999−2021, based on Pléiades, SPOT5, lidar, aerial photographs and ArcticDEM DEMs. A Gaussian Process regression was applied to generate a temporally continuous dataset of surface elevation with a spatial resolution of 15×15 m and temporal resolution of 30 days. The latter was thereafter used for geodetic mass-balance computations for hydrological years (October 1^{st}−September 31^{st}) over four consecutive 5- and 6-year periods in 1999–2021. The obtained mass balance becomes progressively less negative over the analysis period, from -1.83 ± 0.13 m w.e. a^{-1} (1999−2005) to -0.41 ± 0.03 m w.e. a^{-1} (2016−2021).

Three catchments were delineated and analysed to identify local patterns of mass balance. The northern catchment has the highest mass loss, whereas Kötlujökull behaves in a similar manner to the entire ice cap. No difference in mass-balance variability was observed between the three catchments over the two decades.

Although the data and methods presented in this study do not fully resolve for seasonal or annual variability of mass balance, our study highlights the usefulness of mapping of glaciers with multi-temporal DEMs using robust statistics as Gaussian Process. The Gaussian Process brings useful insights in glacier mass balance, particularly at multi-annual time scales.

Acknowledgments

This study was funded by Landsvirkjun (the National Power Company of Iceland). We thank Antoine Rabatel for his valuable comments on an earlier version of the manuscript. Pléiades images were acquired at research price thanks to the CNES DINAMIS programme (https://dinamis.data-terra.org/). This study uses the lidar mapping of the glaciers in Iceland, funded by the Icelandic Research Fund, the Landsvirkjun research fund, the Icelandic Road Administration, the Reykjavík Energy Environmental and Energy Research Fund, the Klima- og Luftgruppen research fund of the Nordic Council of Ministers, the Vatnajökull National Park, the organization Friends of Vatnajökull, LMÍ, IMO, and the UI research fund. EB acknowledges support from the French Space Agency (CNES). We thank the two reviewers and Þorsteinn Þorsteinsson for their constructive comments.

Author contribution

MB and JB carried out the processing and analysis of the data, with inputs from EB, TJ, RH and AD. TJ, JB and AG designed the framework of this project. MB led the writing of the manuscript, with help from all co-authors.

Data availability

The data presented in this study are available at https://doi.org/10.5281/zenodo.7058006 (Bernat *et al.*, 2023). Selected intervals of geodetic mass balance calculated in this study will be uploaded to the World Glacier Monitoring Service.

Landlíkanafkoma Mýrdalsjökuls 1999–2021 Afkomu Mýrdalsjökuls, fjórða stærsta jökuls landsins (520 km^2 árið 2019), hefur verið minni gaumur gefinn en afkomu þriggja stærstu jöklanna, Vatnajökuls, Hofsjökuls og Langjökuls. Hér notum við hæðarlíkön byggð á SPOT5 gervihnattaljósmyndum (2003–2017), leysimælingum úr flugvél (lidar, 2010), Pléiades gervihnattaljósmyndum (2014–2021) og loftmyndum frá 1999, og ArcticDEM landlíkanasafnið

(2010–2018) til þess að meta afkomu Mýrdalsjökuls. Frumúrvinnsla hæðarlíkananna fólst í láréttri og lóðréttri samstillingu, síun og fyllingu í eyður. Síðan var svokallaðri Gaussian tölfræðigreiningu (Gaussian Process, GP) beitt til þess að reikna samfellda tímaröð landlíkana með 15×15 m lárétta upplausn og 30 daga millibili fyrir tímabilið 1999 til 2021. Breytingar í rúmmáli og afkoma voru reiknaðar yfir 5 og 6 ára tímabil og þær túlkaðar með samanburði við mælingar á afkomu Vatnajökuls, Hofsjökuls og Langjökuls. Meðalafkoma Mýrdalsjökuls á tímabilinu 1999–2021 er áætluð $-1{,}23 \pm 0{,}10$ m vatnsgildis á ári, og hefur farið lækkandi að tölugildi frá $-1{,}83 \pm 0{,}13$ m vatnsgildis á ári (1999–2005) til $-0{,}41 \pm 0{,}03$ m vatnsgildis á ári (2016–2021). Greining afkomu fyrir þrjú mismunandi ísflæðisvið á Mýrdalsjökli (norðurhluti jökulsins, suðurhluti jökulsins og Kötlujökull) sýnir nokkurn mun milli svæðanna en svipaðar breytingar með tíma.

REFERENCES

Ágústsson, H., H. Hannesdóttir, Th. Thorsteinsson, F. Pálsson, B. Oddsson and H. Ólafsson 2013. Mass balance of Mýrdalsjökull ice cap accumulation area and comparison of observed winter balance with simulated precipitation. *Jökull* 61, 91–104.

Andreassen, L. M., H. Elvehøy, B. Kjøllmoen and R. V. Engeset 2016. Reanalysis of long-term series of glaciological and geodetic mass balance for 10 Norwegian glaciers. *The Cryosphere* 10(2), 535–552.

Aðalgeirsdóttir, G., E. Magnússon, F. Pálsson, Th. Thorsteinsson, J. M. Belart, T. Jóhannesson, H. Hannesdóttir, O. Sigurðsson, A. Gunnarsson, B. Einarsson, *et al.* 2020. Glacier changes in Iceland from 1890 to 2019. *Frontiers in Earth Science* 8, 523646.

Belart, J. M., E. Magnússon, E. Berthier, A. Gunnlaugsson, F. Pálsson, G. Aðalgeirsdóttir, T. Jóhannesson, Th. Thorsteinsson and H. Björnsson 2020. Mass balance of 14 Icelandic glaciers, 1945–2017: Spatial variations and links with climate. *Frontiers in Earth Science* 8, 163.

Belart, J. M., E. Magnússon, E. Berthier, F. Pálsson, G. Aðalgeirsdóttir and T. Jóhannesson 2019. The geodetic mass balance of Eyjafjallajökull ice cap for 1945–2014: processing guidelines and relation to climate. *J. Glaciology*, 65(251), 395–409.

Bengtsson, L., U. Andrae, T. Aspelien, Y. Batrak, J. Calvo, W. de Rooy, E. Gleeson, B. Hansen-Sass, M. Homleid, M. Hortal, *et al.* 2017. The HARMONIE–AROME model configuration in the ALADIN–HIRLAM NWP system. *Monthly Weather Review* 145(5), 1919–1935.

Bernat, M. and J. M. Belart 2022. Geodetic mass balance of Mýrdalsjökull ice cap, 1999–2021: DEM processing and climate analysis (version v1) [data set]. https://doi.org/10.5281/zenodo.7058006.

Berthier, E., D. Floriciou, A. S. Gardner, N. Gourmelen, L. Jakob, F. Paul, D. Treichler, B. Wouters, J. M. Belart, *et al.* 2023. Measuring glacier mass changes from space? A review. *Reports on Progress in Physics* 86(3), 036801.

Berthier, E., C. Vincent, E. Magnússon, A. Gunnlaugsson, P. Pitte, E. Le Meur, M. Masiokas, L. Ruiz, F. Pálsson, J. M. Belart, *et al.* 2014. Glacier topography and elevation changes derived from Pléiades sub-meter stereo images. *The Cryosphere* 8(6), 2275–2291.

Beyer, R. A., O. Alexandrov and S. McMichael 2018. The Ames Stereo Pipeline: NASA's open source software for deriving and processing terrain data. *Earth and Space Science* 5(9), 537–548.

Björnsson, H. and F. Pálsson 2008. Icelandic glaciers. *Jökull* 58, 365–386.

Björnsson, H., F. Pálsson and M. T. Guðmundsson 2000. Surface and bedrock topography of the Mýrdalsjökull ice cap. *Jökull* 49, 29–46.

Björnsson, H., B. D. Sigurðsson, B. Davíðsdóttir, J. Ólafsson, Ó. S. Ástþórsson, S. Ólafsdóttir, T. Baldursson and T. Jónsson 2018. *Loftslagsbreytingar og áhrif þeirra á Íslandi. Skýrsla vísindanefndar um loftslagsbreytingar (Impacts of climate change in Iceland. Report of the Scientific Committee on Climate Change in Iceland)*. Technical report, Veðurstofa Íslands, Reykjavík.

Crochet, P. 2007. A study of regional precipitation trends in Iceland using a high-quality gauge network and ERA-40. *J. Climate* 20(18), 4659–4677.

Crochet, P. and T. Jóhannesson 2011. A data set of gridded daily temperature in Iceland, 1949–2010. *Jökull* 61, 1–17.

Dehecq, A., A. S. Gardner, O. Alexandrov, S. McMichael, R. Hugonnet, D. Shean and M. Marty 2020. Automated processing of declassified KH-9 Hexagon satellite images for global elevation change analysis since the 1970s. *Frontiers in Earth Science* 8, 566802.

Fischer, M., M. Huss and M. Hoelzle 2015. Surface elevation and mass changes of all Swiss glaciers 1980–2010. *The Cryosphere* 9(2), 525–540.

Girod, L., C. Nuth, A. Kääb, R. McNabb and O. Galland 2017. MMASTER: Improved ASTER DEMs for elevation change monitoring. *Remote Sensing* 9(7), 704.

Gudmundsson, M. T., G. Larsen, A. Höskuldsson and Á. G. Gylfason 2008. Volcanic hazards in Iceland. *Jökull* 58, 251–268.

Hagg, W., C. Mayer, U. Münzer, N. Barbosa, H. M. Schuler and M. Staudacher 2023. Estimating local surface glacier mass balance from migration of the 1918 Katla eruption tephra layer on Sléttjökull, southern Iceland. *Annals of Glaciology* First View. https://doi.org/10.1017/aog.2022.1

Hannesdóttir, H., H. Björnsson, F. Pálsson, G. Aðalgeirsdóttir and S. Guðmundsson 2015. Changes in the southeast Vatnajökull ice cap, Iceland, between 1890 and 2010. *The Cryosphere* 9(2), 565–585.

Hannesdóttir, H., O. Sigurðsson, R. H. Þrastarson, S. Guðmundsson, J. M. Belart, F. Pálsson, E. Magnússon, S. Víkingsson, I. Kaldal and T. Jóhannesson 2020. A national glacier inventory and variations in glacier extent in Iceland from the Little Ice Age maximum to 2019. *Jökull* 70, 1–34.

Hock, R., M. De Woul, V. Radić and M. Dyurgerov 2009. Mountain glaciers and ice caps around Antarctica make a large sea-level rise contribution. *Geoph. Res. Lett.* 36(7), L07501.

Hugonnet, R., F. Brun, E. Berthier, A. Dehecq, E. S. Mannerfelt, N. Eckert and D. Farinotti 2022. Uncertainty analysis of digital elevation models by spatial inference from stable terrain. *IEEE J. Selected Topics in Applied Earth Observations and Remote Sensing* 15, 6456–6472.

Hugonnet, R., R. McNabb, E. Berthier, B. Menounos, C. Nuth, L. Girod, D. Farinotti, M. Huss, I. Dussaillant, F. Brun, *et al.* 2021. Accelerated global glacier mass loss in the early twenty-first century. *Nature* 592(7856), 726–731.

Huss, M. 2013. Density assumptions for converting geodetic glacier volume change to mass change. *The Cryosphere* 7(3), 877–887.

Höhle, J. and M. Höhle 2009. Accuracy assessment of digital elevation models by means of robust statistical methods. *ISPRS J. Photogrammetry and Remote Sensing* 64(4), 398–406.

IPCC 2019. *IPCC Special Report on the Ocean and Cryosphere in a Changing Climate*. [Pörtner, H.-O., D. C. Roberts, V. Masson-Delmotte, P. Zhai, M. Tignor, E. Poloczanska, K. Minten-Beck, A. Alegría, M. Nicolai, A. Okem, J. Petzold, B. Rama, N. M. Weyer (eds.)] Cambridge University, 755 pp.

IPCC 2021. *Climate Change 2021: The Physical Science Basis. Contribution of Working Group I to the Sixth Assessment Report of the Intergovernmental Panel on Climate Change*. Cambridge University Press, Cambridge, United Kingdom, and New York, NY, USA.

Jóhannesson, T., G. Aðalgeirsdóttir, H. Björnsson,black P. Crochet, E. B. Elíasson, S. Guðmundsson, J. Jónsdóttir, H. Ólafsson, F. Pálsson, Ó. Rögnvaldsson, O. Sigurðsson, Á. Snorrason, Ó. G. B. Sveinsson and Th. Thorsteinsson 2007. *Effect of Climate Change on Hydrology and Hydro-Resources in Iceland*. Reykjavík, Orkustofnun, 2007, Reykjavík.

Jóhannesson, T., H. Björnsson, E. Magnússon, S. Guðmundsson, F. Pálsson, O. Sigurðsson, Th. Thorsteinsson and E. Berthier 2013. Ice-volume changes, bias estimation of mass-balance measurements and changes in subglacial lakes derived by lidar mapping of the surface of Icelandic glaciers. *Annals of Glaciology* 54(63), 63–74.

Jóhannesson, T., B. Pálmason, Á. Hjartarson, A. H. Jarosch, E. Magnússon, J. M. Belart and M. T. Gudmundsson 2020. Non-surface mass balance of glaciers in Iceland. *J. Glaciology* 66(258), 685–697.

Korona, J., E. Berthier, M. Bernard, F. Rémy and E. Thouvenot 2009. SPIRIT. SPOT 5 stereoscopic survey of polar ice: Reference Images and Topographies during the fourth International Polar Year (2007–2009). *ISPRS J. Photogrammetry and Remote Sensing* 64(2), 204–212.

Larsen, M., C. Tøttrup, E. Mätzler, B. Naamansen, D. Petersen and K. Thorsøe 2013. A satellite perspective on jökulhlaups in Greenland. *Hydrology Res.* 44(1), 68–77.

Magnússon, E., J. M. Belart, F. Pálsson, H. Ágústsson and P. Crochet 2016. Geodetic mass balance record with rigorous uncertainty estimates deduced from aerial photographs and lidar data–case study from Drangajökull ice cap, NW Iceland. *The Cryosphere* 10(1), 159–177.

Magnússon, E., F. Pálsson, A. H. Jarosch, T. van Boeckel, H. Hannesdóttir and J. M. Belart 2021. The bedrock and tephra layer topography within the glacier filled Katla caldera, Iceland, deduced from dense RES-survey. *Jökull* 71, 39–70.

Mayer, C., J. Jaenicke, A. Lambrecht, L. Braun, C. Völksen, C. Minet and U. Münzer 2017. Local surface mass-balance reconstruction from a tephra layer – a case study on the northern slope of Mýrdalsjökull, Iceland. *J. Glaciology* 63(237), 79–87.

McNabb, R., C. Nuth, A. Kääb and L. Girod 2019. Sensitivity of glacier volume change estimation to DEM void interpolation. *The Cryosphere* 13(3), 895–910.

Nawri, N., B. Pálmason, G. N. Petersen, H. Björnsson and S. Þorsteinsson 2017. *The ICRA atmospheric reanalysis project for Iceland*. Icelandic Meteorological Office, Report 2017-005.

Noël, B., G. Aðalgeirsdóttir, F. Pálsson, B. Wouters, S. Lhermitte, J. M. Haacker and M. R. van den Broeke 2022. North Atlantic cooling is slowing down mass loss of Icelandic glaciers. *Geoph. Res. Lett.* 49(3), e2021GL095697.

Nuth, C. and A. Kääb 2011. Co-registration and bias corrections of satellite elevation data sets for quantifying glacier thickness change. *The Cryosphere* 5(1), 271–290.

Porter, C., P. Morin, I. Howat, M. Noh, B. Bates, K. Peterman, S. Keesey, *et al.* 2018. *Arctic DEM*. Harvard Dataverse, 1.

Pálsson, F. 2022a. *Afkomu- og hraðamælingar á Langjökli jökulárið 2021–22*. Reykjavík, Landsvirkjun, Institute of Earth Sciences, University of Iceland, LV-2022-053.

Pálsson, F. 2022b. *Vatnajökull. Mass balance, meltwater drainage and surface velocity of the glacial year 2021–22*. Reykjavík, Landsvirkjun, Institute of Earth Sciences, Univ. Iceland, LV-2022-054.

Pálsson, F., A. Gunnarsson, H. S. Pálsson and S. Steinþórsson 2021a. *Afkomu- og hraðamælingar á Langjökli jökulárið 2019–20*. Reykjavík, Landsvirkjun, Institute of Earth Sciences, Univ. Iceland, LV-2021-004.

Pálsson, F., A. Gunnarsson, H. S. Pálsson and S. Steinþórsson 2021b. *Vatnajökull: Mass balance, meltwater drainage and surface velocity of the glacial year 2019–20*. Reykjavík, Landsvirkjun, Institute of Earth Sciences, University of Iceland, LV-2021-003.

Pálsson, F., S. Guðmundsson, H. Björnsson, E. Berthier, E. Magnússon, S. Guðmundsson and H. H. Haraldsson 2012. Mass and volume changes of Langjökull ice cap, Iceland, 1890 to 2009, deduced from old maps, satellite images and in situ mass balance measurements. *Jökull* 62, 81– 96.

Raup, B. H., S. J. S. Khalsa, R. L. Armstrong, W. A. Sneed, G. S. Hamilton, F. Paul, F. Cawkwell, M. J. Beedle, B. P. Menounos, *et al.* 2014. Quality in the GLIMS glacier database. In: Kargel, J. S., G. Leonard, M. P. Bishop, A. Kääb and B. H. Raup (eds.). *Global Land Ice Measurements from Space* 163–182. Springer, Heidelberg.

Rolstad, C., T. Haug and B. Denby 2009. Spatially integrated geodetic glacier mass balance and its uncertainty based on geostatistical analysis: application to the western Svartisen ice cap, Norway. *J. Glaciology* 55(192), 666–680.

Shean, D., S. Bhushan, E. Berthier, C. Deschamps-Berger, S. Gascoin and F. Knuth 2021. *Chamoli disaster post-event 2-m dem composite (february 10–11, 2021) and difference map (1.0)* [data set]. Zenodo.

Shean, D. E., O. Alexandrov, Z. M. Moratto, B. E. Smith, I. R. Joughin, C. Porter and P. Morin 2016. An automated, open-source pipeline for mass production of digital elevation models (DEMs) from very-high-resolution commercial stereo satellite imagery. *ISPRS J. Photogrammetry and Remote Sensing* 116, 101–117.

Sveinsson, Ó. G. B. 2016. *Energy in Iceland: Adaptation to Climate Change*. UNU-FLORES Policy Briefs, United Nations University Institute for Integrated Management of Material Fluxes and of Resources, Dresden.

Thorsteinsson, Th., T. Jóhannesson, O. Sigurðsson and B. Einarsson 2017. *Afkomumælingar á Hofsjökli 1988–2017 (Mass balance measurements on Hofsjökull 1988–2017)*. Icelandic Meteorological Office, Report 2017-016, 85 pp.